1D to 2D Self Assembly of Cyclic Peptides

Ignacio Insua and Javier Montenegro*

Centro Singular de Investigación en Química Biolóxica e Materiais Moleculares (CIQUS), Departamento de Química Orgánica, Universidade de Santiago de Compostela, 15782, Spain.

ABSTRACT: Despite recent developments in two-dimensional self-assembly, most supramolecular 2D materials are assembled by tedious methodologies, with complex surface chemistry and small sizes. We here report D/L-alternating cyclic peptides that undergo one-dimensional self-assembly into amphiphilic nanotubes, which subsequently arrange as tubular bilayers to form giant nanosheets in the mesoscale. Reversible transitions between the assembled, dispersed and aggregated states of these nanosheets can be triggered by external stimuli. The characteristic flexibility, defined chemical topology and length scale of these nanosheets set a clear distinction between this new supramolecular architecture and previously reported 2D nanostructures. The sequential 1D-to-2D self-assembly of peptides described here provides a conceptually new approach to achieve two-dimensional materials with hierarchical organisation. These giant nanosheets represent one of the largest 2D supramolecular materials ever made, with potential application as long-range molecular transporters, responsive surfaces and (bio)sensors.

INTRODUCTION

The different levels of protein structure define the spatial distribution of the amino acids involved in the non-covalent interactions that define protein shape and function.[1] Thus, a protein's primary sequence encodes the information for the hydrogen-bonded patterns of its secondary structure (*e.g.* α-helix or β-sheet). The spatial arrangement of these secondary motifs yields tertiary protein assemblies, whose controlled aggregation leads to the assembly of the final quaternary protein oligomers. Since the early years of supramolecular chemistry, artificial molecular designs have been extensively studied to mimic the hierarchical assembly of proteins with controlled topology.[2-10] Recent advances to control the topology and function of synthetic supramolecular systems include the application of chirality,[11] mechanical stress[12] and oscillating assembly mechanisms.[13]

The unique chemical reactivity and physical properties of two-dimensional (2D) molecular allotropes has opened new and exciting opportunities in chemistry, nanotechnology and materials science.[14,15] To this end, a myriad of inorganic and organic bottom-up approaches towards 2D covalent and supramolecular materials have been developed over the last decade.[15] Directed DNA and protein folding at the nanoscale have allowed the preparation of 2D biocompatible materials.[3,16-18] In particular, peptide-based scaffolds that undergo 2D self-assembly[19,20] include peptides,[21-24] proteins,[21,25,26] peptoids[27,28] and derivatives thereof,[29,30] which have found applications in sensing,[27,31] catalysis[24] and molecular biology.[22] However, despite remarkable progress in synthetic supramolecular systems, a synthetic small molecule with different pre-programmed levels of hierarchical self-assembly and adaptive behaviour has remained elusive.

Herein, we report the design principles of the first cyclic peptide capable of undergoing sequential 1D-to-2D self-assembly in aqueous medium to produce dynamic and giant two-dimensional supramolecular structures in the mesoscale. The primary amino acid sequence of this cyclic peptide codifies all the chemical information needed for the adoption of the secondary folded β-sheet motif, which gives rise to the corresponding nanotubes that were further associated as crystalline, yet dynamic, 2D nanosheets. These ultrathin supramolecular assemblies constitute one of the largest fully organic 2D structures ever assembled in solution. Microscopy, spectroscopy, X-ray scattering and computational models were employed to demonstrate the crystalline structure of the nanosheets and their defined chemical topology. The resulting 2D assemblies respond to external stimuli (*i.e.* temperature and pH) by reversibly changing conformation between disassembled, aggregated and extended states. The new hierarchical architecture described here, constituted by hollow tubular ensembles with adjustable nanolumens, opens new avenues for the bottom-up assembly of aqueous 2D supramolecular materials with controlled topology in the mesoscale.

RESULTS

Supramolecular design

Cyclic peptides with an even number of amino acids and alternating D/L-chirality stack on top of one another to form hollow self-assembled cyclic peptide nanotubes

(SCPNs).[32,33] In this architecture, the length and nature of the primary sequence dictate the diameter and the surface chemistry of the resulting nanotube. The synthetic simplicity and self-assembly mechanism of cyclic peptides allow an exceptional level of geometrical control that is amplified along the final nanotubular ensemble. Therefore, since their discovery, SCPNs have shown their outstanding potential as functional size-selective ion channels, molecular switches, tubular composites, antibiotics, charge transport systems and drug delivery vehicles.[34-38]

The cyclic peptide design described here was based on the pioneering work by Ghadiri *et al.*,[32] where the self-assembly of cyclic peptides bearing glutamic acids was triggered by acidification and carboxylate protonation, which resulted in the neutralisation of charge repulsions and thus the self-assembly of 1D nanotubular bundles.[39] The assembly of peptide nanotubes was confirmed to be controlled by the formation of cooperative and enthalpy-driven hydrogen-bonded networks.[40,41] As previously reported, the incorporation of leucine residues into neutral cyclic peptide monomers afforded remarkably static and thermodynamically stable nanotube bundles.[40] In these nanotubes, the packing of hydrophobic side chains restricted the competition of water for the hydrogen bonds between peptide backbones, resulting in SCPNs that were stable from below freezing temperatures to boiling water.[40] On this basis, we hypothesised that SCPNs exploiting hydrophobic interactions but assembled from peptide monomers in their ionised state would weaken the attractive forces along the nanotubes by charge repulsions,[42] thus creating a more dynamic supramolecular network where stimuli-responsiveness and adaptive behaviour could emerge.

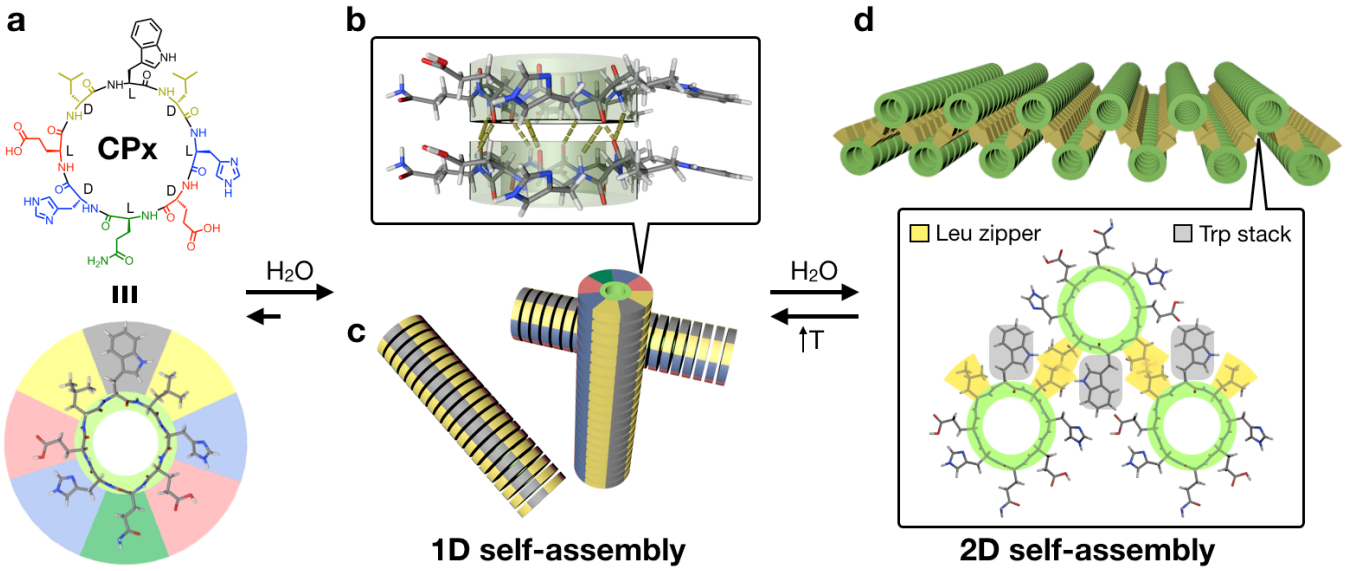

Figure 1. Proposed model for the sequential 1D-to-2D self-assembly of cyclic peptide **CPx**. (a) Primary amino acid sequence of **CPx** and colour coding. (b) Secondary parallel β-sheet conformation between **CPx** backbones within nanotubes stabilised via eight hydrogen bonds (dashed lines). (c) Tertiary 1D self-assembly of **CPx** as amphiphilic peptide nanotubes with hydrophobic (Leu-Trp-Leu in yellow-grey) and hydrophilic (Glu-His-Gln in red-blue-green) surfaces. (d) 2D self-assembly of **CPx** into nanosheets comprising nanotube bilayers with hydrophobic cores –composed of Leu zippers (yellow) and Trp stacks (grey)– and polar residues on their surface.

Following these principles, we designed cyclic peptide X (**CPx**), which consists of eight residues with alternating D/L-chirality arranged into four distinct domains: i) a hydrophobic tripeptide comprising a tryptophan flanked by two leucines (Leu-Trp-Leu); ii) two hydrophilic ionisable domains on either side of the peptide ring including the pH-sensitive glutamic acid and histidine (Glu, His); iii) and a neutral hydrophilic glutamine (Gln) opposite to the tryptophan in the hydrophobic domain (Figure 1). In solution, **CPx** would adopt a parallel β-sheet secondary structure to afford an amphiphilic nanotube, which would have to self-organise into a nanotubular bilayer to bury its hydrophobic face from the aqueous environment (Figure 1c-d). At physiological pH (7.4), the surface of the tubular ensemble will have a highly anionic character due to the theoretical deprotonation degree (>99.9%) of the glutamic acids ($pK_a \approx 4.2$) and the neutrality (>96%) of histidine residues ($pK_a \approx 6.0$).[43] Therefore, the resulting amphiphilic nanotubes should pack into a hydrophobic bilayer, where the shifting of one peptide nanotube to stagger the top and bottom layers would give rise to stabilising leucine zippers and π-π stacks of tryptophan indoles (Figure 1d). The strongly anionic surface of the resulting 2D architecture would prevent the aggregation of the individual layers, which would be further stabilised by intermolecular hydrogen

bonding between histidine and glutamine side chains. Furthermore, the presence of pH-sensitive residues and the repulsive anionic character of the system could allow the dynamic remodelling of the supramolecular structure (soluble ↔ 1D ↔ 2D) with pH and/or temperature. The design principles encoded in the primary amino acid sequence of **CPx** would thus allow the controlled one-dimensional stacking of cyclic peptide monomers, the subsequent assembly of the nanotubes into two-dimensional supramolecular nanosheets, and their controlled and reversible stimuli-responsive behaviour.

Hierarchical 1D-to-2D peptide self-assembly

Cyclic peptide **CPx** was prepared by conventional solid-phase peptide synthesis as previously reported (see Supporting Information).[39] The self-assembly of **CPx** was initially studied at physiological pH (20 mM Na_2HPO_4 buffer, pH 7.4), where theoretically over 96% of peptide molecules should bear two negative charges. To start at maximal monomer solubility, a solution of **CPx** (100 μM) was heated at 80°C for 1.5 hours and let to cool down to room temperature to promote the assembly of the system. To visualise the resulting supramolecular structures, solutions of **CPx** were stained with the fluorescent probe thioflavin-T (10 μM), which is known to intercalate β-sheets resulting in enhanced fluorescence due to the probe's planarisation.[44] The corresponding fluorescence micrographs revealed remarkably large and flat nanosheets, with lateral dimensions in the high micron range (*e.g.* 260 x 50 μm) and surfaces of up to 15,000 μm² (Figure 2 and S13). These nanosheets were transparent and flexible, as evidenced by their resistance to folding and wrinkling (Figure 2a-b). Despite being assembled in solution, the integrity of the nanosheets was preserved after drying the samples for microscopy analysis (Figure 2), which demonstrates the remarkable stability of this supramolecular 2D network outside its solvated state.

Scanning-transmission electron microscopy (STEM) confirmed the formation of transparent 2D structures, reminiscent of single graphene layers (Figure 2c-d).[45] STEM micrographs revealed the presence of aligned nanotubes in areas with fragmented sheets, indicative of backward 2D-to-1D disassembly of the supramolecular system (Figure S14). Sonication of **CPx** nanosheets allowed the isolation of peptide nanotubes and nanotubular bundles, with no evidence of surviving nanosheets (Figure S15). However, when this sonicated sample was left overnight at room temperature, the 2D nanosheets formed again from the nanotubes spontaneously (Figure S16). Furthermore, only 1D nanotube bundles were found by STEM during nanosheet annealing at 80°C (Figure S17), and dynamic light scattering (DLS) showed a clear increase in the hydrodynamic diameter of the sample when cooling from 80°C to 20°C, indicative of a 1D-to-2D transition (Figure S18). These results supported peptide nanotubes as the building blocks for the 2D supramolecular architecture and were consistent with a sequential 1D-to-2D self-assembly pathway (Figure 1). As in similar crystalline peptide nanotubes,[46] the high structural order of these 2D ensembles allowed the emergence of light birefringence on drop-cast **CPx** nanosheets (Figure 2e-f). Cross-polarised optical micrographs showed illuminated nanosheets when the light polarisers cancelled each other at 90°, displaying different brightness depending on their folding and orientation.

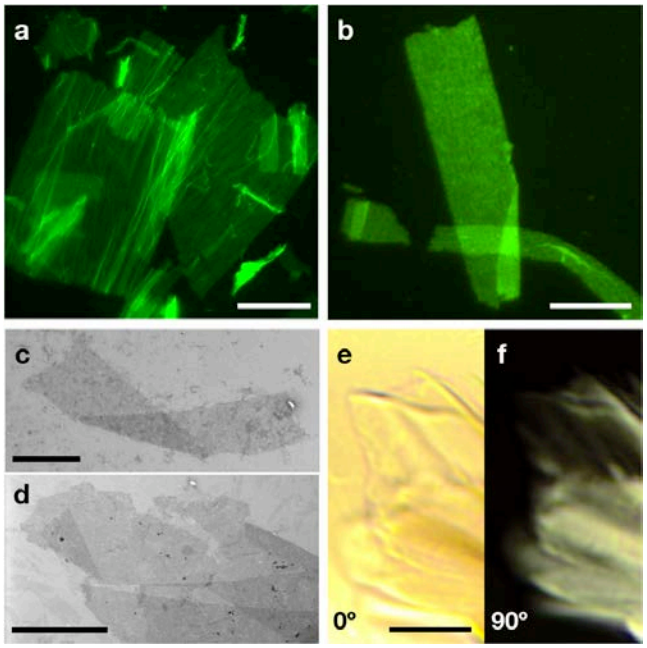

Figure 2. Microscopic characterisation of **CPx** supramolecular nanosheets. (a-b) Epifluorescence micrographs of nanosheets (**CPx** 100 μM, pH 7.4, annealing: i. 80°C/1.5 h; ii. R.T./1 h) in presence of thioflavin-T (10 μM). Scale bar = 50 μm (a) and 20 μm (b). (c-d) Scanning transmission electron microscopy (STEM) of nanosheets. Scale bars = 2 μm. (e-f) Cross-polarised optical micrographs at 0° (full illumination, e) and 90° (full cancellation, f) angles between polarisers. Scale bar = 15 μm.

The self-assembly of **CPx** nanosheets was then investigated across different peptide concentrations and annealing temperatures. Firstly, peptide concentration was screened in the micromolar range, showing no evidence of sheets at the lowest concentration tested (5 μM) and the progressive appearance of an amorphous background and disassembly of nanosheets at the two highest concentrations (250 and 500 μM) (Figure S19). Peptide concentrations in the intermediate micromolar range (20-100 μM) showed the formation of defined nanosheets with increasing size and abundance with higher peptide concentration. Next, the effect of temperature on the nanosheet annealing process was studied (Figure S20). Unheated peptide samples showed few small nanosheets together with polydisperse peptide aggregates. In contrast, heated samples showed larger nanosheets with increasing temperatures, which was consistent with the thermodynamic evolution of the system towards the 2D assembled nanosheets.

Dynamic behaviour of CPx nanosheets

The effect of temperature on pre-assembled nanosheets was investigated by measuring thioflavin-T emission during heating and cooling steps.[44] Fluorescence spectroscopy revealed the quenching of thioflavin-T emission with temperature, indicating the progressive disassembly of the supramolecular nanosheets (Figure 3a). From a dispersed state at 80°C, fluorescence emission was spontaneously recovered at room temperature in *ca.* 40 min, which suggests the completion of the re-assembly process (Figure 3b). Epifluorescence microscopy of heated samples confirmed the complete disappearance of thioflavin-stained nanosheets, which were recovered at room temperature in a disassembly/assembly cycle that could be repeated as many times as desired (Figure 3c).

To explore the pH dependence of this system, samples of anionic **CPx** nanosheets prepared at room temperature and pH 7.4 were acidified to the pK_a of histidine (pH 6.0, protonation: ~ 50% His and ~ 0% Glu). The generation of positive charges in about half of the histidine imidazoles caused the collapse of the anionic nanosheets due to the enhanced electrostatic attraction between cyclic peptide monomers (Figure 3d-e). Subsequent pH cycles within physiological range (7.4 ↔ 6.0) confirmed the reversible transition between peptide aggregates and extended 2D nanosheets (Figure 3e). Further acidification of the sample to the pK_a of glutamic acid (pH 4, protonation: ~ 100% His, ~ 50% Glu), still showed the presence of electrostatically collapsed peptide aggregates. However, acidification until **CPx** acquired full positive charge (pH 2.8, protonation: ~ 100% His, ~ 100% Glu) restored the electrostatic repulsion between **CPx** monomers and thus the nanosheet configuration of the system (Figure 3f and S21). Interestingly, nanosheets at pH 2.8 presented higher aspect ratios than those found at pH 7.4, which could be an effect of the different counterions and attractive-repulsive forces present at these two ionisation states. Despite the persistence of certain kinetic aggregates formed during the pH cycle, the same structural transitions were observed when the pH was reversed to physiological levels, and the 2D nanosheets were recovered at pH 7.4 (Figure 3f). Additionally, heated samples allowed the removal of the peptide aggregates formed after the morphological transitions during pH cycles (Figure S22).

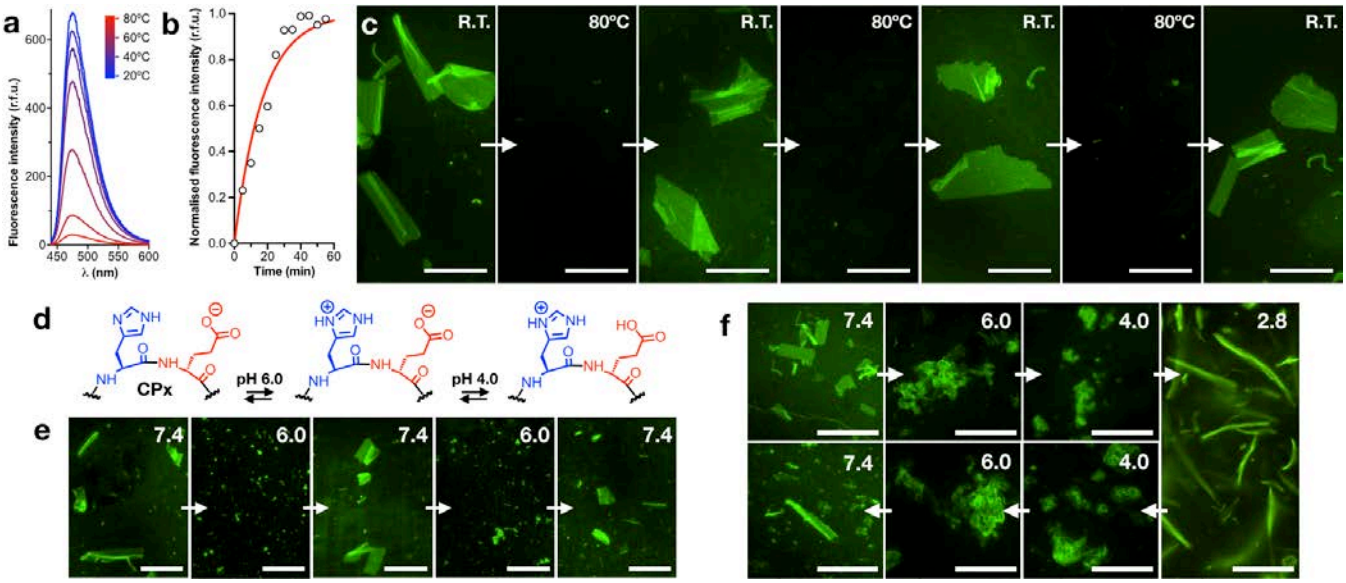

Figure 3. Dynamic behaviour of **CPx** supramolecular nanosheets. (a) Fluorescence emission of thioflavin-T (ThT) in a **CPx** solution heated from 20 to 80°C. (b) Relative fluorescence emission of ThT in a **CPx** solution cooled from 80°C to 20°C. (c) Epifluorescence micrographs of a **CPx** solution during successive heating (80°C/1.5 h) and cooling (R.T./1 h) steps. The first 'R.T.' image had been previously heated (80°C/1.5 h). Scale bars = 30 μm. (d) Simplified structure of **CPx** showing its three ionisation states. (e-f) Epifluorescence micrographs of *unheated* **CPx** solutions prepared at pH 7.4 and sequentially adjusted to different pH values (top-right insets). Scale bars = 50 μm. In all cases [**CPx**] = 100 μM and [ThT] = 10 μM.

Structural characterisation of CPx nanosheets

The spectroscopic FT-IR analysis of **CPx** nanosheets showed a band at 3267 cm^{-1} (N-H stretching) and the characteristic bands at 1674 and 1627 cm^{-1} for amide I, and at 1540 cm^{-1} for amide II, which were consistent with amide bonds compromised in parallel β-sheets (Figure S23).[47,48] Additionally, the circular dichroism (CD) spectrum of the nanosheets showed a positive Cotton effect located at 224 nm (Figure S24), almost identical to the profile previously reported for indole stacks in tryptophan-rich peptide hairpins.[49] The CD spectrum recorded at 80°C showed the same profile –only weaker– as that of 2D nanosheets (Figure S24), which confirms the disassembly of the system to its 1D state with heat, and

not to an achiral monomeric state. A control peptide of **CPx** with the two leucines replaced for alanines (**CPxAla**) only assembled aggregated fibres and few undefined sheets under the same conditions, which further supports the key role of leucine zippers in the stabilisation of the ordered 2D packing of nanotubes (Figure S25). Therefore, FT-IR, CD and control experiments supported the parallel β-sheet configuration and tryptophan stacking in the nanosheet architecture (Figure 1).

To further prove the importance of **CPx**'s sequence for nanosheet assembly, two more structural variations were explored: **CPx-Glu** (Figure S26) and **CPx-His** (Figure S27) have neutral glutamines replacing the two glutamic acids and histidines of the native structure, respectively. Neither of these two new variants was able to assemble nanosheets, which confirmed the critical importance of the imidazole and the carboxylate groups in the hydrophilic domain, and hence the design principles described in this manuscript.

Atomic force microscopy (AFM) of **CPx** nanosheets deposited on mica revealed a constant height of 3.2 nm along the cross-section of the 2D ensemble (Figure 4a). As previously observed by STEM, the sonication of nanosheet suspensions allowed the imaging of transition states corresponding to laterally associated nanotubes. Individual nanotubes exhibited heights of *ca*. 1.6 nm by AFM (Figure 4b), which were consistent with a nanotubular bilayer forming the 3.2 nm thick nanosheets. The internal structure of **CPx** nanosheets was studied by wide angle X-ray scattering (WAXS) from a supported dry suspension of nanosheets (see Methods). WAXS analysis showed scattering signals at 4.8 and 16.7 Å, which can be correlated to the axial spacing of cyclic peptides along the nanotubes and the distance between nanotube plains in the proposed 2D arrangement, respectively (Figure 4c). Together, the dimensions found by AFM and WAXS are in agreement with the values reported in the literature[40,47,50] for other cyclic D/L-peptide nanotubes.[51]

Molecular geometry optimisations were conducted using density functional theory (DFT) calculations to model the arrangement of **CPx** units based on previously reported crystal structures of cyclic peptide nanotubes (see Methods).[47] The energy minimisation of a **CPx** dimer in parallel β-sheet conformation showed an axial spacing between peptide rings of 4.7 Å, which is in agreement with the WAXS results and the expected distance for a hydrogen bonded β-sheet (Figure 4d). Furthermore, the calculated dimer also showed additional hydrogen bonding and face-to-face π-π stacking between superimposed glutamine and tryptophan residues, respectively. Repeats of **CPx** units from the calculated structure arranged in the proposed bilayer architecture (Figure 1d) afforded spacings matching the experimental values observed by AFM and WAXS (Figure 4d). In summary, the FT-IR analysis, CD, AFM, WAXS and DFT calculations confirmed the proposed tubular bilayer architecture with intercalated peptide units, which are stabilised by leucine zippers between adjacent nanotubes from each layer (Figure 1d and 4d).[47]

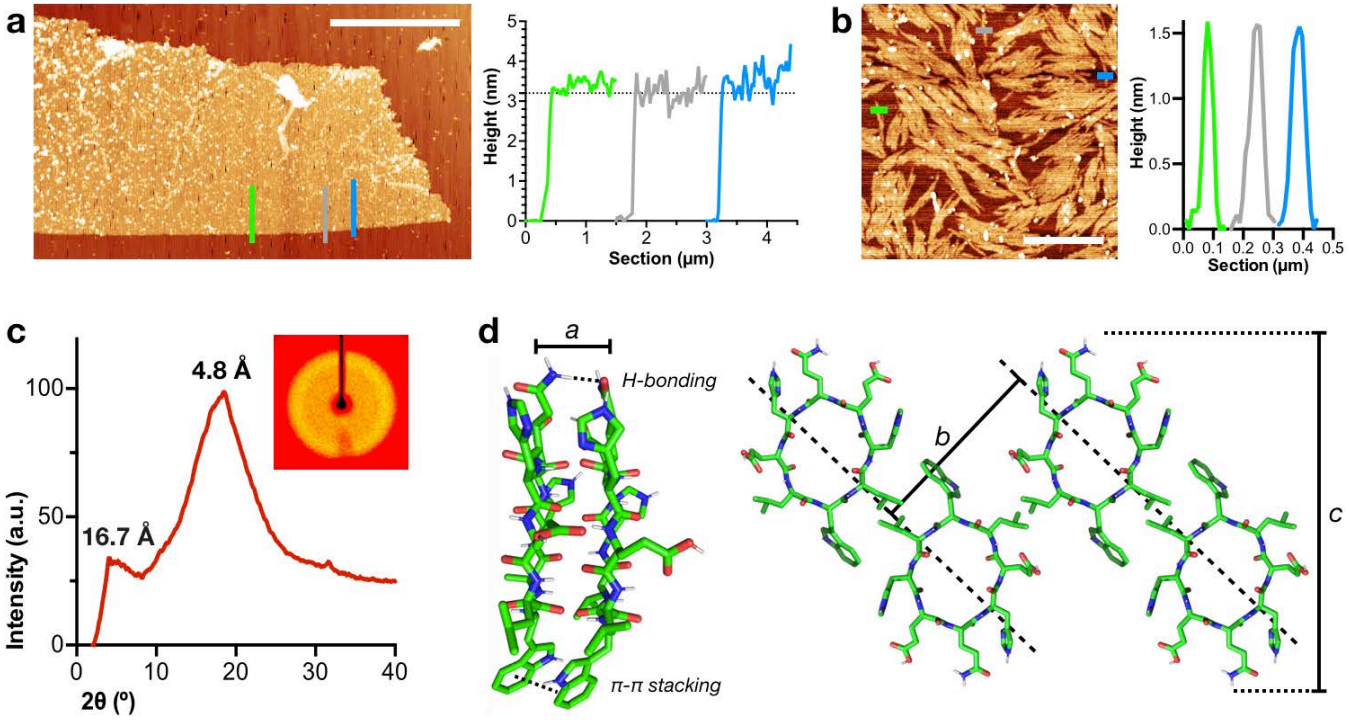

Figure 4. Structural characterisation of **CPx** supramolecular nanosheets. (a-b) Atomic force microscopy (AFM) images and height profiles of a nanosheet (a) and a sonicated sample of sheets (b) deposited on mica. Scale bar = 4 μm (a) and 1 μm (b). (c) Wide angle X-ray scattering (WAXS) profile of a dry sample of nanosheets. (d) Density functional theory (DFT)-minimised **CPx** stacked dimer (left) and DFT-minimised **CPx** monomers in the proposed 2D arrangement (right) highlighting the distances

found by AFM and WAXS: a = 4.8 Å, b = 16.7 Å, c = 3.2 nm. Scattering plains established by the 2D nanotubular bilayer are indicated with dashed lines.

DISCUSSION

The supramolecular nanosheets reported here constitute a conceptually new 2D material in terms of structure, properties and design. Unlike many 2D allotropes, **CPx** nanosheets are flexible and self-assembled in aqueous solution without complex formulation steps (*e.g.* exfoliation or interfacial nucleation).[15] Indeed, other methods (*e.g.* surface-assisted peptide assembly[52] and organic-inorganic composites[53]) have produced giant 2D supramolecular structures, but **CPx** nanosheets stand out as one of the largest fully organic supramolecular 2D materials self-assembled in solution. This 2D structure showed dynamic behaviour in response to temperature and pH, which caused remarkable long-range (*i.e.* micrometric) yet reversible transitions between different supramolecular states, while preserving the memory of the system to reassemble in 2D (Figure 3). Temperature-dependent experiments are consistent with the 2D arrangement of **CPx** as the thermodynamic product of the self-assembly process. Spectroscopic CD and FT-IR analysis confirmed the formation of parallel β-sheets and tryptophan stacks, which would imply the establishment of leucine zippers to stabilise the hydrophobic packing of the nanosheets. Indeed, control experiments with a peptide where the leucines were replaced by alanines (**CPxAla**) confirmed the key role of leucines in the 2D supramolecular network. pH titrations also demonstrated the importance of glutamic acids and the overall anionic charge of **CPx** to assemble defined and extended 2D nanosheets, which result from an interplay between attractive forces (*i.e.* H-bonding and hydrophobic effects) and repulsive Coulombic interactions. Likewise, control peptides without glutamic acids (**CPx-Glu**) or histidines (**CPx-His**) did not assemble supramolecular nanosheets, which proves the importance of the hydrophilic domain of **CPx** for its two-dimensional self-assembly. Design-wise, this work sets a stepping-stone in the hierarchical control of self-assembly across different dimensions by repurposing supramolecular 1D cyclic peptide nanotubes for subsequent 2D association. Although STEM, DLS and CD experiments prove the 1D-to-2D self-assembly pathway during nanosheet annealing, an equilibrium of **CPx** units between the monomer, 1D and 2D states could take place after annealing. Also, the high aspect ratio of certain nanosheets suggests distinct growth rates in 1D and 2D, as expected from the different interactions involved in each elongation and the higher stability of 1D nanotubes to heat.

CONCLUSIONS

This work presents the first two-dimensional self-assembly of D/L-alternating cyclic peptides by sequential 1D-to-2D supramolecular polymerisation. The primary amino acid sequence of the cyclic peptide described here (**CPx**) encoded all the chemical information required to establish the secondary β-sheets that arranged into tertiary 1D nanotubes, which subsequently self-assembled into 2D supramolecular nanosheets. These nanosheets constitute one of the largest 2D supramolecular materials ever assembled in aqueous solution, reaching lateral dimensions in the high micron-range and a constant nanometre thickness. The adaptive response to external stimuli such as pH and temperature allowed the dynamic disassembly, aggregation and reassembly of this new 2D material in the mesoscale. Overall, we have introduced the design principles for a simple cyclic peptide that undergoes hierarchical and controlled self-assembly across two dimensions. This innovative strategy will promote the development of a new class of 2D hollow supramolecular systems, which could have strong implications in size-selective ion and molecular storage, micron-scale transporters and biocompatible membranes that respond to their medium.

METHODS

Peptide synthesis and characterisation. Cyclic peptides were synthesised following procedures previously reported by our group (see Supporting Information for details).

2D supramolecular assembly of cyclic peptides. A solution of cyclic peptide (*e.g.* **CPx**; 100 μM) in 20 mM phosphate buffer at pH 7.4 was gently vortexed for 10 s and then incubated in the dark at 80°C for 1.5 h without shaking. Then, the sample was stored at room temperature (R.T.) for 1 h to assemble the 2D supramolecular nanosheets. Samples to be imaged by fluorescence microscopy also contained thioflavin-T (10 μM) at the start of the heating process. *Unheated* samples were prepared likewise, only skipping the sequential heating (80°C/1.5 h) and cooling (R.T./1 h) steps. Unless specified, all nanosheets were prepared with one heating-cooling cycle. Samples annealed at different temperatures followed the heating-cooling cycle indicated here, only the heating step took place at the temperatures indicated in Figure S20.

Microscopic imaging of nanosheets and nanotubes. For epifluorescence and cross-polarised microscopy, 10 μL of nanosheet suspension were spotted on glass slides and the sample was left to dry completely at room temperature in the dark before imaging. For STEM, a nanosheet suspension was diluted 100-fold with MilliQ water, then 5 μL spotted on a TEM grid and the sample was imaged once dry without washing nor staining. For AFM, 5 μL of a nanosheet sample were cast on mica, left to dry, and then gently washed with MilliQ water (5 μL x5). Nanotube samples were imaged likewise using a nanosheet sample diluted 10-fold with MilliQ

water, only this time the sample was sonicated for 30 min before deposition.

Heating-cooling (dis)assembly of nanosheets. For thioflavin-T emission experiments (Ex=430 nm; Em=440-600 nm), an *unheated* nanosheet sample containing thioflavin-T (10 μM) was heated from 20°C to 80°C in 10°C steps with 5 min of stabilisation at each T point (Figure 3a). After the final measurement (*i.e.* 80°C), the instrument was set at 20°C and fluorescence emission was monitored over time as the sample cooled down (Figure 3b; data normalised to the maximum emission observed).

pH-dependent nanosheet morphology. The pH of an *unheated* nanosheet sample containing thioflavin-T (10 μM) was adjusted with 100 mM HCl or NaOH by gentle mixing to avoid foaming. At each pH step, 10 μL of this *unheated* sample were spotted on glass slides and imaged by epifluorescence microscopy once dry (Figure 3e-f). Cycles between pH 7.4 and 6.0 were studied with heating-cooling cycles (i. 80°C/1.5 h; ii. R.T./1 h) at each pH step before imaging (Figure S22).

WAXS measurements. Sample scattering was measured at 2 degrees in the phi axis, with an exposure time of 300 s per frame, and the Debye rings were integrated with the Bruker SAINT software package using a narrow-frame algorithm. Two samples were recorded from a mounting loop, one just containing paratone oil as background contribution (*i.e.* blank), and the second one composed of a dry sample of supramolecular nanosheets suspended in paratone. The integrated data without the background contribution (Figure 4c) was obtained from the subtraction of the former sample to the latter with the software HighScore Plus.

DFT calculations. For the calculated molecular geometries, the core cyclic peptide backbone was constructed using the crystal structure reported by Chalmers *et al.*,[47] whose amino acid side chains were modified to match those of **CPx**, and the cyclic peptide backbone was kept frozen during the geometry optimisation. All the calculated molecular geometries were first optimised using the semi-empirical method PM6.[54] The monomer and dimers geometries were then further optimised using the M06-2X functional and the 6-31G* all-electron basis set,[55] as implemented in Gaussian09/D.01.[56] In all cases, the absence of imaginary frequencies confirmed that the found geometries corresponds to a local energy minimum. The calculated structure is provided as Cartesian coordinates in the native *XYZ* file format.

ASSOCIATED CONTENT

Supporting Information

The Supporting Information is available free of charge on the ACS Publications website at DOI: xxxxxxxxx

Supporting figures and chemical characterisation (PDF)

Calculated molecular geometries (XYZ)

AUTHOR INFORMATION

Corresponding author

* javier.montenegro@usc.es

ORCID

Ignacio Insua: 0000-0002-5134-9910

Javier Montenegro: 0000-0001-6503-2095

Notes

The authors declare no competing financial interest.

ACKNOWLEDGEMENTS

This work was partially supported by the Spanish Agencia Estatal de Investigación (AEI) [SAF2017-89890-R], the Xunta de Galicia (ED431C 2017/25, 2016-AD031 and Centro Singular de Investigación de Galicia accreditation 2016–2019, ED431G/09), the ISCIII (RD16/0008/003), and the European Union (European Regional Development Fund – ERDF). I.I. thanks the European Commission for a Marie Curie fellowship (MSCA-IF-2018-843332) and the Spanish AEI for a Juan de la Cierva - Formación fellowship (FJCI-2017-31795). J.M. received a Ramón y Cajal (RYC-2013-13784), an ERC Starting Investigator Grant (DYNAP-677786) and a Young Investigator Grant from the HFSP (RGY0066/2017). We thank Dr. Eugenio Solla, Prof. Juan Granja, Dr. Julian Bergueiro, Dr. Andreas Vargas Jentzsch and Dr. Mark J. van Raaij for helpful discussions. We also thank Dr. Bergueiro for Figure 1 and Dr. Vargas Jentzsch for assistance with DFT calculations.

REFERENCES AND NOTES

(1) Creighton, T. E. *Proteins: Structures and molecular properties*, 2nd ed.; Wiley: New York, **1992**.

(2) Aida, T.; Meijer, E. W.; Stupp, S. I. Functional supramolecular polymers. *Science* **2012**, *335*, 813–817.

(3) Ljubetič, A.; Gradišar, H.; Jerala, R. Advances in design of protein folds and assemblies. *Curr. Opin. Chem. Biol.* **2017**, *40*, 65–71.

(4) De Santis, E.; Ryadnov, M. G. Peptide self-assembly for nanomaterials: The old new kid on the block. *Chem. Soc. Rev.* **2015**, *44*, 8288–8300.

(5) Krieg, E.; Bastings, M. M. C.; Besenius, P.; Rybtchinski, B. Supramolecular polymers in aqueous media. *Chem. Rev.* **2016**, *116*, 2414–2477.

(6) Lehn, J.-M. Perspectives in chemistry-Aspects of adaptive chemistry and materials. *Angew. Chem. Int. Ed.* **2015**, *54*, 3276–3289.

(7) Grzybowski, B. A.; Fitzner, K.; Paczesny, J.; Granick, S. From dynamic self-assembly to networked chemical systems. *Chem. Soc. Rev.* **2017**, *46*, 5647–5678.

(8) del Barrio, J.; Liu, J.; Brady, R. A.; Tan, C. S. Y.; Chiodini, S.; Ricci, M.; Fernández-Leiro, R.; Tsai, C.-J.; Vasileiadi, P.; Di Michele, L.; *et al*. Emerging two-dimensional crystallization of cucurbit[8]uril complexes: From supramolecular polymers to nanofibers. *J. Am. Chem. Soc.* **2019**, *141*, 14021–14025.

(9) Matern, J.; Dorca, Y.; Sánchez, L.; Fernández, G. Revising complex supramolecular polymerization under kinetic and thermodynamic control. *Angew. Chem. Int. Ed.* **2019**, *doi: 10.1002/anie.201905724*.

(10) Vázquez-González, V.; Mayoral, M. J.; Chamorro, R.; Hendrix, M. M. R. M.; Voets, I. K.; González-Rodríguez, D. Noncovalent synthesis of self-assembled nanotubes through

decoupled hierarchical cooperative processes. *J. Am. Chem. Soc.* **2019**, *141*, 16432–16438.
(11) Garcia, A. M.; Iglesias, D.; Parisi, E.; Styan, K. E.; Waddington, L. J.; Deganutti, C.; De Zorzi, R.; Grassi, M.; Melchionna, M.; Vargiu, A. V.; *et al*. Chirality effects on peptide self-assembly unraveled from molecules to materials. *Chem* **2018**, *4*, 1862–1876.
(12) Fredy, J. W.; Méndez-Ardoy, A.; Kwangmettatam, S.; Bochicchio, D.; Matt, B.; Stuart, M. C. A.; Huskens, J.; Katsonis, N.; Pavan, G. M.; Kudernac, T. Molecular photoswitches mediating the strain-driven disassembly of supramolecular tubules. *Proc. Natl. Acad. Sci. U.S.A.* **2017**, *114*, 11850–11855.
(13) Leira-Iglesias, J.; Tassoni, A.; Adachi, T.; Stich, M.; Hermans, T. M. Oscillations, travelling fronts and patterns in a supramolecular system. *Nat. Nanotechnol.* **2018**, *13*, 1021–1027.
(14) Zhu, J.; Yang, C.; Lu, C.; Zhang, F.; Yuan, Z.; Zhuang, X. Two-dimensional porous polymers: From sandwich-like structure to layered skeleton. *Acc. Chem. Res.* **2018**, *51*, 3191–3202.
(15) Dong, R.; Zhang, T.; Feng, X. Interface-assisted synthesis of 2D materials: Trend and challenges. *Chem. Rev.* **2018**, *118*, 6189–6235.
(16) Jun, H.; Zhang, F.; Shepherd, T.; Ratanalert, S.; Qi, X.; Yan, H.; Bathe, M. Autonomously designed free-form 2D DNA origami. *Sci. Adv.* **2019**, 5, eaav0655.
(17) He, Y.; Chen, Y.; Liu, H.; Ribbe, A. E.; Mao, C. Self-assembly of hexagonal DNA two-dimensional (2D) arrays. *J. Am. Chem. Soc.* **2005**, *127*, 12202–12203.
(18) Bai, W.; Sargent, C. J.; Choi, J.-M.; Pappu, R. V.; Zhang, F. Covalently-assembled single-chain protein nanostructures with ultra-high stability. *Nat. Commun.* **2019**, *10*, 3317.
(19) Liu, L.; Klausen, L. H.; Dong, M. Two-dimensional peptide based functional nanomaterials. *Nano Today* **2018**, *23*, 40–58.
(20) Zhang, W.; Yang, P. 2D Bio-nanostructures fabricated by supramolecular self-assembly of protein, peptide, or peptoid. *Adv. Compos. Hybrid Mater.* **2018**, *2*, 201–213.
(21) Merg, A. D.; Touponse, G.; van Genderen, E.; Zuo, X.; Bazrafshan, A.; Blum, T.; Hughes, S.; Salaita, K.; Abrahams, J. P.; Conticello, V. P. 2D crystal engineering of nanosheets assembled from helical peptide building blocks. *Angew. Chem. Int. Ed.* **2019**, *131*, 13641-13646.
(22) Dai, B.; Li, D.; Xi, W.; Luo, F.; Zhang, X.; Zou, M.; Cao, M.; Hu, J.; Wang, W.; Wei, G.; *et al*. Tunable assembly of amyloid-forming peptides into nanosheets as a retrovirus carrier. *Proc. Natl. Acad. Sci. U.S.A.* **2015**, *112*, 2996–3001.
(23) Jiang, T.; Xu, C.; Liu, Y.; Liu, Z.; Wall, J. S.; Zuo, X.; Lian, T.; Salaita, K.; Ni, C.; Pochan, D.; *et al*. Structurally defined nanoscale sheets from self-assembly of collagen-mimetic peptides. *J. Am. Chem. Soc.* **2014**, *136*, 4300–4308.
(24) Jang, H.-S.; Lee, J.-H.; Park, Y.-S.; Kim, Y.-O.; Park, J.; Yang, T.-Y.; Jin, K.; Lee, J.; Park, S.; You, J. M.; *et al*. Tyrosine-mediated two-dimensional peptide assembly and its role as a bio-inspired catalytic scaffold. *Nat. Commun.* **2014**, *5*, 3665.
(25) Brodin, J. D.; Carr, J. R.; Sontz, P. A.; Tezcan, F. A. Exceptionally stable, redox-active supramolecular protein assemblies with emergent properties. *Proc. Natl. Acad. Sci. U.S.A.* **2014**, *111*, 2897–2902.
(26) Knowles, T. P. J.; Oppenheim, T. W.; Buell, A. K.; Chirgadze, D. Y.; Welland, M. E. Nanostructured films from hierarchical self-assembly of amyloidogenic proteins. *Nat. Nanotechnol.* **2010**, *5*, 204–207.
(27) Nam, K. T.; Shelby, S. A.; Choi, P. H.; Marciel, A. B.; Chen, R.; Tan, L.; Chu, T. K.; Mesch, R. A.; Lee, B.-C.; Connolly, M. D.; *et al*. Free-floating ultrathin two-dimensional crystals from sequence-specific peptoid polymers. *Nat. Mater.* **2010**, *9*, 454–460.
(28) Jin, H.; Jiao, F.; Daily, M. D.; Chen, Y.; Yan, F.; Ding, Y.-H.; Zhang, X.; Robertson, E. J.; Baer, M. D.; Chen, C.-L. Highly stable and self-repairing membrane-mimetic 2D nanomaterials assembled from lipid-like peptoids. *Nat. Commun.* **2016**, *7*, 12252.
(29) Lin, Y.; Penna, M.; Thomas, M. R.; Wojciechowski, J. P.; Leonardo, V.; Wang, Y.; Pashuck, E. T.; Yarovsky, I.; Stevens, M. M. Residue-specific solvation-directed thermodynamic and kinetic control over peptide self-assembly with 1D/2D structure selection. *ACS Nano* **2019**, *13*, 1900–1909.
(30) Lewandowska, U.; Zajaczkowski, W.; Corra, S.; Tanabe, J.; Borrmann, R.; Benetti, E. M.; Stappert, S.; Watanabe, K.; Ochs, N. A. K.; Schaeublin, R.; *et al*. A triaxial supramolecular weave. *Nat. Chem.* **2017**, *9*, 1068–1072.
(31) Battigelli, A.; Kim, J. H.; Dehigaspitiya, D. C.; Proulx, C.; Robertson, E. J.; Murray, D. J.; Rad, B.; Kirshenbaum, K.; Zuckermann, R. N. Glycosylated peptoid nanosheets as a multivalent scaffold for protein recognition. *ACS Nano* **2018**, *12*, 2455–2465.
(32) Ghadiri, M. R.; Granja, J. R.; Milligan, R. A.; McRee, D. E.; Khazanovich, N. Self-assembling organic nanotubes based on a cyclic peptide architecture. *Nature* **1993**, *366*, 324–327.
(33) Khazanovich, N.; Granja, J. R.; McRee, D. E.; Milligan, R. A.; Ghadiri, M. R. Nanoscale tubular ensembles with specified internal diameters. Design of a self-assembled nanotube with a 13-Å pore. *J. Am. Chem. Soc.* **1994**, *116*, 6011–6012.
(34) Fuertes, A.; Juanes, M.; Granja, J. R.; Montenegro, J. Supramolecular functional assemblies: Dynamic membrane transporters and peptide nanotubular composites. *Chem. Commun.* **2017**, 53, 7861–7871.
(35) Montenegro, J.; Ghadiri, M. R.; Granja, J. R. Ion channel models based on self-assembling cyclic peptide nanotubes. *Acc. Chem. Res.* **2013**, *46*, 2955–2965.
(36) Li, M.; Ehlers, M.; Schlesiger, S.; Zellermann, E.; Knauer, S. K.; Schmuck, C. Incorporation of a non-natural arginine analogue into a cyclic peptide leads to formation of positively charged nanofibers capable of gene transfection. *Angew. Chem. Int. Ed. Engl.* **2016**, 55, 598–601.
(37) Cuerva, M.; García-Fandiño, R.; Vázquez-Vázquez, C.; López-Quintela, M. A.; Montenegro, J.; Granja, J. R. Self-assembly of silver metal clusters of small atomicity on cyclic peptide nanotubes. *ACS Nano* **2015**, *9*, 10834–10843.
(38) Montenegro, J.; Vázquez-Vázquez, C.; Kalinin, A.; Geckeler, K. E.; Granja, J. R. Coupling of carbon and peptide nanotubes. *J. Am. Chem. Soc.* **2014**, *136*, 2484–2491.
(39) Méndez-Ardoy, A.; Granja, J. R.; Montenegro, J. pH-triggered self-assembly and hydrogelation of cyclic peptide nanotubes confined in water micro-droplets. *Nanoscale Horiz.* **2018**, *3*, 391–396.
(40) Hartgerink, J. D.; Granja, J. R.; Milligan, R. A.; Ghadiri, M. R. Self-assembling peptide nanotubes. *J. Am. Chem. Soc.* **1996**, *118*, 43–50.
(41) Ghadiri, M. R.; Kobayashi, K.; Granja, J. R.; Chadha, R. K.; McRee, D. E. The structural and thermodynamic basis for the formation of self-assembled peptide nanotubes. *Angew. Chem. Int. Ed. Engl.* **1995**, *34*, 93–95.
(42) Besenius, P.; Portale, G.; Bomans, P. H. H.; Janssen, H. M.; Palmans, A. R. A.; Meijer, E. W. Controlling the growth and shape of chiral supramolecular polymers in water. *Proc. Natl. Acad. Sci. U.S.A.* **2010**, *107*, 17888–17893.
(43) Nelson, D. L.; Cox, M. M.; Cox, M. M. *Lehninger principles of biochemistry*, 5th ed. W H Freeman & Company: New York, **2008**.
(44) Wolfe, L. S.; Calabrese, M. F.; Nath, A.; Blaho, D. V.; Miranker, A. D.; Xiong, Y. Protein-induced photophysical changes to the amyloid indicator dye thioflavin T. *Proc. Natl. Acad. Sci. U.S.A.* **2010**, *107*, 16863–16868.
(45) Tung, V. C.; Allen, M. J.; Yang, Y.; Kaner, R. B. High-throughput solution processing of large-scale graphene. *Nat. Nanotechnol.* **2009**, *4*, 25–29.

(46) Rubin, D. J.; Amini, S.; Zhou, F.; Su, H.; Miserez, A.; Joshi, N. S. Structural, nanomechanical, and computational characterization of D,L-cyclic peptide assemblies. *ACS Nano* **2015**, *9*, 3360–3368.
(47) Silk, M. R.; Newman, J.; Ratcliffe, J. C.; White, J. F.; Caradoc-Davies, T.; Price, J. R.; Perrier, S.; Thompson, P. E.; Chalmers, D. K. Parallel and antiparallel cyclic D/L peptide nanotubes. *Chem. Commun.* **2017**, *53*, 6613–6616.
(48) Zou, Y.; Li, Y.; Hao, W.; Hu, X.; Ma, G. Parallel β-sheet fibril and antiparallel β-sheet oligomer: New insights into amyloid formation of hen egg white lysozyme under heat and acidic condition from FTIR spectroscopy. *J. Phys. Chem. B* **2013**, *117*, 4003–4013.
(49) Cochran, A. G.; Skelton, N. J.; Starovasnik, M. A. Tryptophan zippers: Stable, monomeric β-hairpins. *Proc. Natl. Acad. Sci. U.S.A.* **2001**, *98*, 5578–5583.
(50) Rapaport, H.; Kim, H. S.; Kjaer, K.; Howes, P. B.; Cohen, S.; Als-Nielsen, J.; Reza Ghadiri, M.; Leiserowitz, L.; Lahav, M. Crystalline cyclic peptide nanotubes at interfaces. *J. Am. Chem. Soc.* **1999**, *121*, 1186–1191.
(51) Depending on amino acid composition and/or substitution, cyclic peptide nanotubes display crystalline lattices with axial and lateral spacings of 4.5-4.8 Å and 15-20 Å, respectively.
(52) Lee, J.; Choe, I. R.; Kim, N.-K.; Kim, W.-J.; Jang, H.-S.; Lee, Y.-S.; Nam, K. T. Water-floating giant nanosheets from helical peptide pentamers. *ACS Nano* **2016**, *10*, 8263–8270.
(53) Cortecchia, D.; Neutzner, S.; Srimath Kandada, A. R.; Mosconi, E.; Meggiolaro, D.; De Angelis, F.; Soci, C.; Petrozza, A. Broadband emission in two-dimensional hybrid perovskites: The role of structural deformation. *J. Am. Chem. Soc.* **2016**, *139*, 39–42.
(54) Stewart, J. J. P. Optimization of parameters for semiempirical methods V: Modification of NDDO approximations and application to 70 elements. *J. Mol. Model.* **2007**, *13*, 1173–1213.
(55) Zhao, Y.; Truhlar, D. G. The M06 suite of density functionals for main group thermochemistry, thermochemical kinetics, noncovalent interactions, excited states, and transition elements: Two new functionals and systematic testing of four M06-class functionals and 12 other functionals. *Theor. Chem. Acc.* **2007**, *120*, 215–241.
(56) Frisch, M. J.; Trucks, G. W.; Schlegel, H. B.; Scuseria, G. E.; Robb, M. A.; Cheeseman, J. R.; Scalmani, G.; Barone, V.; Mannucci, B.; Petersson, G. A. *Gaussian 09, Revision D.01*; Gaussian, Inc., Wallingford CT, **2009**.

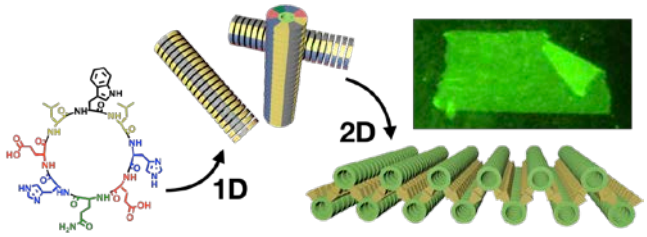
1D
2D